SUPPORTING INFORMATION

The electromagnets

Each electromagnet consisted of a coil surrounding a central pole piece which replaces the permanent magnets. The core was constructed of 1018 low-carbon steel and the coil was wound with 1900 turns of 18 American Wire Gage (AWG) copper wire. A diagram of the coils and the magnetic circuit showing microscope field of view (region of interest, ROI) is provided in Fig. 2(a).

CTV software

Significant improvements in the interface of the CTV software have also been implemented. The CTV software consists of two main parts: an image acquisition part and an image processing and data analysis part. An overall outline of how the host computer controls the hardware involved is shown in Fig. 9. With GPIB and RS-232 programmable interface cards, the CTV software allows the user to set up the desired magnetic energy gradient, S_m, based on previously determined calibration curves of magnetic energy gradient and current. In addition, the software can also control the Harvard syringe pump allowing automatic delivery of samples into the CTV viewing region. A Gauss meter (Model 6010, F.W. Bell, Orlando, Florida) placed near to the testing channel is included to allow the user to monitor or record the magnetic induction, B_0, during experiments.

Significant improvements have also been implemented in the actual operation of the CTV program. A flow chart outlining the program algorithm is provided in Fig. 9. The current version, written in C++, runs on a Gateway E-4400 host computer with 512 Mbytes of RAM that can store in excess of 600 frames and an 80 Gbytes hard drives for image archiving. Consecutive images can be captured by a Cohu CCD camera (Model 4915, San Diego, CA) with the sampling frequency of 30 f s^{-1}. The images from the camera were digitized by an M-Vision 1000 PCI 8-bit Video Digitizer (MuTech, Billerica, MA) with resolution of 640 × 480 pixels. The magnification of the microscope produces the spatial resolution of the system in the present experiment of 2.7 μm per pixel. The current version allows the user to choose different frame rates under different operating conditions, including field on and off, thereby allowing the magnetically induced velocity, u_m, and the settling velocity, u_g, to be determined, respectively, for the same particle.

The second part of the CTV software is for image processing and data analysis. It consists of five parts: 1) image pre-processing, 2) cell (or particle) identification, 3) cell tracking, 4) cell velocity calculation, and 5) statistical data analysis. Because of the noisy background and small size of cells, it is almost impossible to distinguish the moving cells from a single image. To overcome this difficulty a dynamic mean-field method is utilized which enables the background to be removed from the series of images. Other commonly used image processing functions are included in this latest version of the CTV code such as erode, dilate, edge, negative, contrast, contour, and threshold. In addition to the raw images, this new version also can read in and convert to different formatted images such as bmp, tiff, jpg, and png. It is also able to make digital format videos (avi) for further studies, presentations, or reports.

Calibration and zeroing of electromagnet

The high magnetic fields generated in the CTV system (on the order of 1 tesla) results in a residual magnetic field in the steel pole pieces of the CTV instrument. This is not a problem when permanent magnets are used, but results in significant uncertainty in the actual field strength when the electromagnet is repeatedly turned on and off. Consequently, an electric current switching system was incorporated which results in a reversal of the current, and thereby the polarity, of the applied magnetic field, leading to the desired steel pole piece demagnetization. Since the intent of the addition of the electromagnet was to be able to accurately vary the magnetic energy gradient in an automatic manner, a relationship of current to magnetic field, and correspondingly, the magnetic energy gradient, was needed. This spatial field calibration was developed using a Hall effect probe attached to the Gauss meter mounted on a stage of a programmable syringe pump (Model 71-2102, Harvard PHD 2000, Hollison, MA). A computer controlled auto-calibration program was also developed and used to measure the magnetic field along the x- axis and y = 0 plane of symmetry (Fig. 2(a)). The probe was initially aligned with the top edge of the pole piece (x = 0) and measurements were recorded at intervals of 0.25 mm from 4 mm to 14 mm. The magnetic flux density, B_0, was measured as a function of the electric current in the coils of the electromagnet and recorded directly into the host computer. At each x position, measurements were made at currents ranging from -0.08 A to 5.0 A at intervals of 0.2 A through each coil.

Calibration of CTV electromagnet

Fig. 11(a) shows plots of the experimentally measured magnetic induction, B_0, as a function of the Gauss meter probe position on the magnet's plane of symmetry (y = 0, Fig. 2(a)) along x axis, for different settings of the electric current powering the electromagnet, ranging from -0.08 to 5.0 A. These experimental measurements, squared, were then fitted to a cubic polynomial curve at each current, Fig. 11(b). Calculations of dB_0^2/dx as a function of position spanning the CTV region of interest, ROI (x = 4 to14 mm, y = 0) and the current powering the electromagnet, were made as shown in Fig. 12. The ROI of the CTV was centered at 8.5 mm, the flattest region of the curves, and therefore a region of the nearly constant S_{m} that best approximates the isodynamic condition of the magnetic field. At x = 8.5 mm, a sixth-order polynomial was used to fit dB_0^2/dx data to the current. From the expression for S_m in eqn (2), the dependence of S_m on the electric current powering the electromagnets, at the center of the ROI, is then calculated and presented in Fig. 3.

A computer screen image after the CTV program has tracked particle settling trajectories (in the vertical direction) and the trajectories for the same particles after the magnetic field was switched on (in the horizontal direction) is shown in Fig. 2(b).

Error Analysis

The saturation magnetization, $M_{s,ave}$ presented in Table 1 is an average value for the PSM-magnetic nanoparticles complex. It was calculated with the assumption that the susceptibility contribution from the microsphere and that of the solution is negligible compared to that of the nanoparticles. We estimated the error of this assumption, as well as made an estimate of the value of the M_{sat} of the magnetic particles themselves. This analysis is based on the full expression for the magnetophoretic mobility, eqn (7). First, inspection of eqn (7) indicates that the term χ_f (-9.05×10^{-6} for the PBS buffer) is small as compared to $\mu_0 M_s/B_0$ (which ranges from 0.003 to 0.16). To obtain this range of $\mu_0 M_s/B_0$, the range of B_0 in the experiments presented in Fig. 8(a-c) was from 0.03 to 1.03 T. Secondly, the MM of PSM, $m_{\mu s}$, in PBS solution is small (2.64×10^{-6} mm^3 T^{-1}A^{-1}s^{-1}, Fig. 5(b)) as compared to that of the labeled PSM (Fig. 8(a)), which justified its omission in eqn (7). Overall, the diamagnetic effects of the PSM in PBS were at least three orders of magnitude smaller than the superparamagnetic effects of the nanoparticles attached to the PSM, which justified their not being included in the expression in eqns (9) and (13).

Legends for Figures

Fig. 9 Diagram depecting the flow of information from CTV host computer to various hardware components.

Fig. 10 Flow chart for the operation of the CTV program.

Fig. 11 Experimentally measured B_0 field (a) and calculated B_0^2 (b) on the plane of symmetry y = 0, along x axis, at 27 different values of the electric current powering the electromagnet coils (I = -0.08, 0.00, 0.20, 0.40, …. , 4.80, 5.00 A).

Fig. 12 Values of dB_0^2/dx on the plane of symmetry y = 0 over a range of x covering the CTV region of interest (ROI), as a function of the electric current in the coils. (Note 27 different current values were tried, from -0.08 A, 0.00 A to 5.00 A at intervals of 0.20 A.)

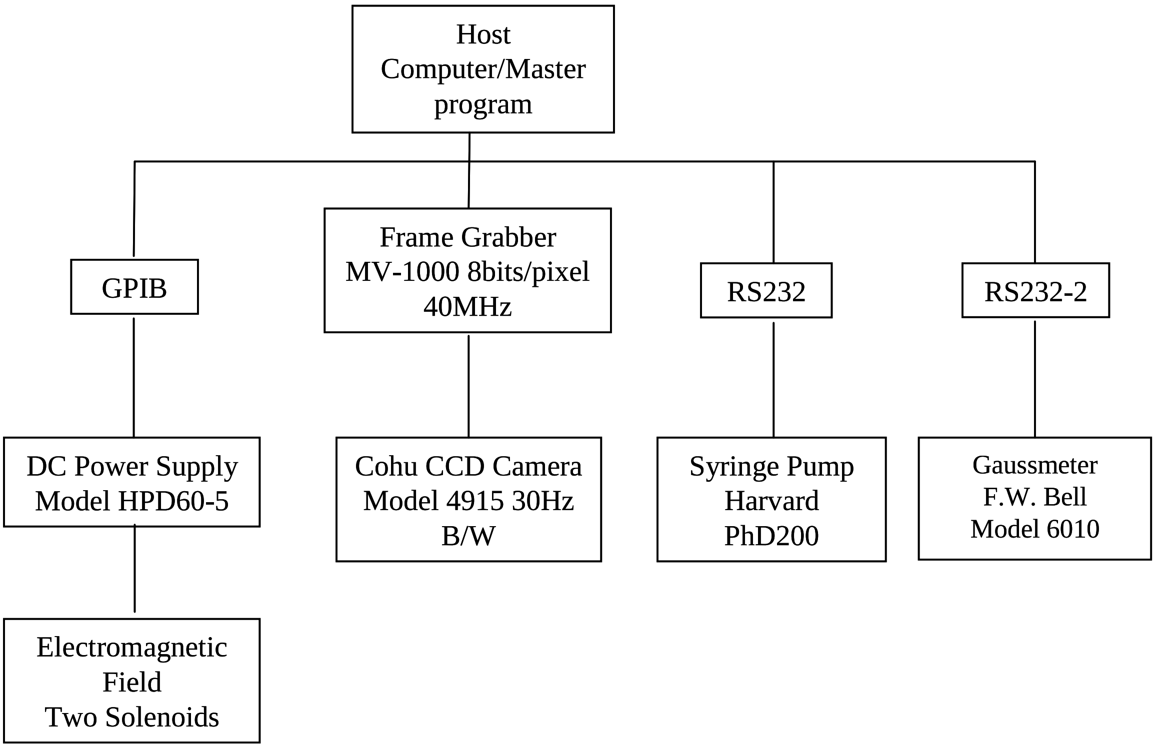

Fig. 9 Diagram depecting the flow of information from CTV host computer to various hardware components.

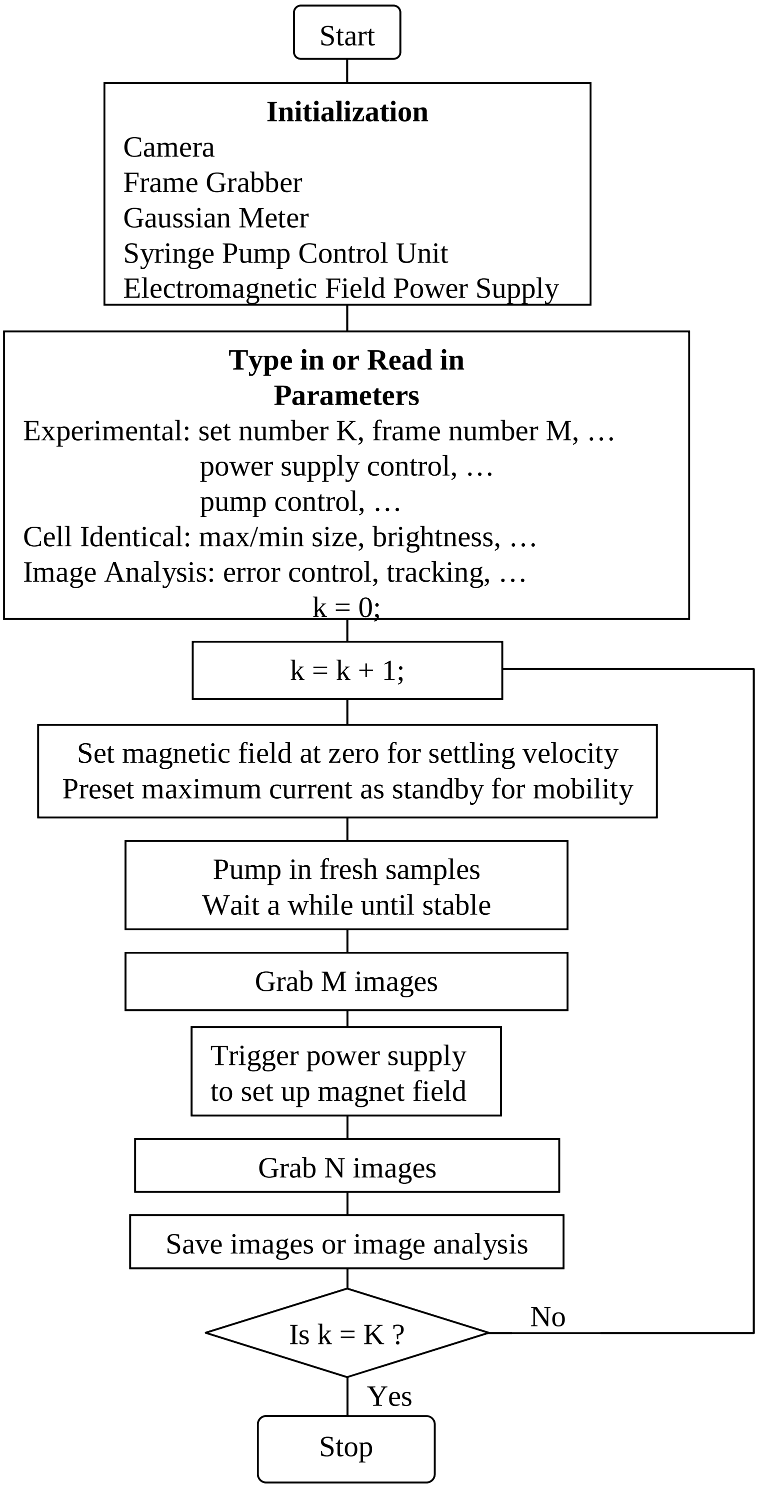

Fig. 10 Flow chart for the operation of the CTV program.

(a)

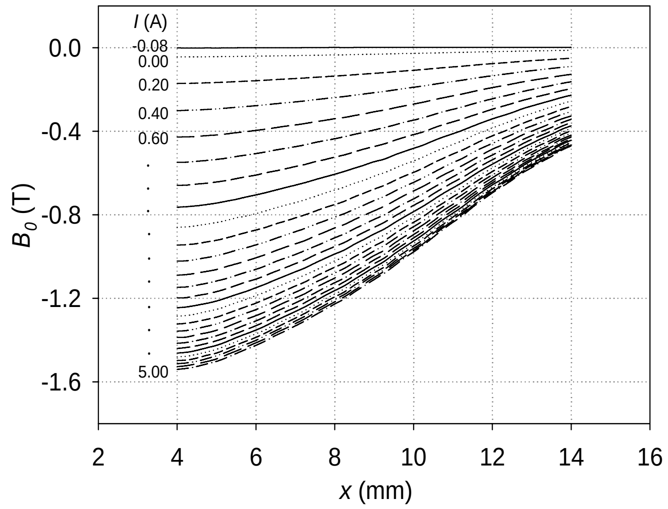

(b)

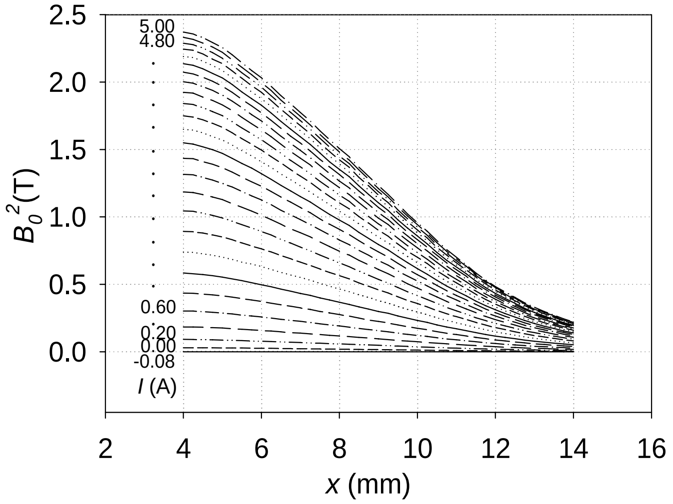

Fig. 11 Experimentally measured B_0 field (a) and calculated B_0^2 (b) on the plane of symmetry $y = 0$, along x axis, at 27 different values of the electric current powering the electromagnet coils (I = -0.08, 0.00, 0.20, 0.40, …. , 4.80, 5.00 A).

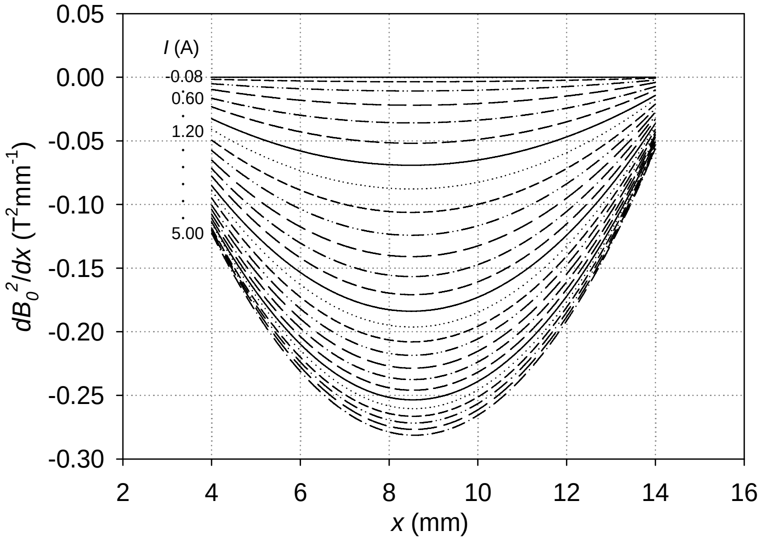

Fig. 12 Values of dB_0^2/dx on the plane of symmetry $y = 0$ over a range of x covering the CTV region of interest (ROI), as a function of the electric current in the coils. (Note 27 different current values were tried, from -0.08 A, 0.00 A to 5.00 A at intervals of 0.20 A.)